Identification of New Target DCTPP1 for Colorectal Cancer Therapy with the Natural Small-molecule Inhibitors Regulating Metabolic Reprogramming

Li Feng,[†,#] Xinjia Wang,[†,#] Xinrui Guo,[†] Liyuan Shi,[†] Shihuang Su,[†] Xinjing Li,[†] Jia Wang,[§] Ninghua Tan,*[,†] Yi Ma,*[,‡] and Zhe Wang*[,†]

[†] State Key Laboratory of Natural Medicines, School of Traditional Chinese Pharmacy, China Pharmaceutical University, Nanjing 211198, People's Republic of China;

[‡] State Key Laboratory of Natural Medicines, School of Engineering, China Pharmaceutical University, Nanjing 211198, China;

[§] School of Pharmacy, Nanjing Medical University, Nanjing 211166, China.

[#] These authors contributed equally to this work.

https://doi.org/10.26434/chemrxiv-2024-g54bp **ORCID:** https://orcid.org/0000-0002-7854-8207 Content not peer-reviewed by ChemRxiv. **License:** CC BY-NC-ND 4.0

ABSTRACT

Colorectal cancer (CRC) is one of the most common malignant tumors. Identification of new effective drug targets for CRC and exploration of bioactive small-molecules are clinically urgent. The human dCTP pyrophosphatase 1 (DCTPP1) is a newly identified pyrophosphatase regulating the cellular nucleotide pool but remains unexplored as potential target for CRC treatment. Here, twelve unprecedented chemical architectures terpene-nonadride heterodimers (**1**–**12**) and their monomers (**13**–**20**) were isolated from endophyte *Bipolaris victoriae* S27. Compounds **1**–**12** represented the first example of terpene-nonadride heterodimers, in which nonadride monomers of **1** and **2** were also first example of 5/6 bicyclic nonadrides. A series of assays showed that **2** could repress proliferation and induce cell cycle arrest, apoptotic and autophagic CRC cell death *in vitro* and *in vivo*. Clinical cancer samples data revealed that DCTPP1 was a novel target associated with poor survival in CRC. DCTPP1 was also identified as a new target protein of **2**. Mechanistically, compound **2** bound to DCTPP1, inhibited its enzymatic activity, intervened with amino acid metabolic reprogramming, and exerted anti-CRC activity. Our study demonstrates that DCTPP1 was a novel potential biomarker and therapeutic target in CRC, and **2** was the first natural anti-CRC drug candidate targeting DCTPP1.

Keywords: *Bipolaris victoriae*, terpene-nonadride heterodimers, structure elucidation, human dCTP pyrophosphatase 1, amino acid metabolic reprogramming

https://doi.org/10.26434/chemrxiv-2024-g54bp **ORCID:** https://orcid.org/0000-0002-7854-8207 Content not peer-reviewed by ChemRxiv. **License:** CC BY-NC-ND 4.0

Colorectal cancer (CRC) is the third cancer and the second deadliest cancer in the world.[1] Currently, surgery and chemotherapy are the most common treatments for CRC. The molecular targeted therapy, whose concept was first proposed in early 1900s and extended to cancer treatment in 1988,[2] can directly inhibit cancerous cell proliferation, differentiation, and migration. Molecular targeted therapy is a new optional effective approach for CRC patients, and the first FDA-approved targeted drug for CRC was cetuximab (EGFR) in 2004, followed by bevacizumab (VEGF) in the same year.[3] Since then, emerging molecular targeted drugs for CRC have come into the market successively, including recently FDA-approved adagrasib, one small-molecule covalent inhibitors of KRAS.[4] Although enormous advances in chemotherapy, the prognosis of CRC is still unsatisfying due to the CRC patients with metastatic lesions, drug target resistance, immune system disorder, serious side effects, and individual differences.[5] Therefore, there is an urgent clinical need to identify novel targets and develop new potential therapeutic drugs for CRC.

The human dCTP pyrophosphatase 1 (DCTPP1), belongs to MazG-like nucleoside triphosphate pyrophosphatase superfamily and is a newly identified pyrophosphatase, which could regulate the cellular nucleotide pool though catalyzing the hydrolysis of canonical and non-canonical deoxynucleoside triphosphates (dNTPs) to the corresponding deoxynucleoside monophosphates (dNMPs) and diphosphate.[6] Recent evidences indicated that DCTPP1 is closely related to the development and progression of tumors,[7] in which it is highly expressed. Overexpression of DCTPP1 promotes cell invasion, migration, and proliferation, inhibits cell apoptosis, and enables cancer cells

https://doi.org/10.26434/chemrxiv-2024-g54bp **ORCID:** https://orcid.org/0000-0002-7854-8207 Content not peer-reviewed by ChemRxiv. **License:** CC BY-NC-ND 4.0

to acquire a high phenotype such as anti-apoptosis and extracellular matrix degradation.[8] Moreover, DCTPP1 is a typical positive regulator of the Wnt pathway, which is crucial for embryonic development and cell proliferation.[9] Besides, as an important part of nucleotide metabolism, DCTPP1 might affect energy metabolism, including amino acid metabolism.[10] Currently, only a few of DCTPP1 inhibitors have been reported, including triptolide, terpenoid epoxide, benzimidazole, and triazolothiadiazole.[11] Therefore, DCTPP1 might be an important biomarker and target for tumor therapy, and development of DCTPP1 inhibitors is very promising.

Small molecules, major participants in targeted therapy, are a group of molecules with the molecular weight less than 900 Da. Among them, natural products (NPs) are bioactive substances mainly isolated from plants, fungi, bacteria, and marine organisms. NPs and their derivatives have been increasingly considered in the design of anti-cancer drugs due to their various structural features and biological activities, as well as low toxicities and side effects. Approximately 50 % of the currently used anticancer drugs were directly or indirectly obtained from NPs.[12] Dimeric or hybrid compounds usually possess high structural complexity, chemical diversity, and significant bioactivity, such as taxol, ancistrocladine,[13] sarglaoxolane,[14] and krishnadimer.[15] Remarkably, these kinds of compounds could also exhibit stronger bioactivities than their monomers.[16] Besides, as for structural optimization, hybridization have been a powerful concept to increase the pharmacological efficacy of known drugs molecules and overcome drug resistance.[17] Although natural dimeric compounds were considered as uncommon components, they have already been extensively obtained from organisms and plants.[18]

https://doi.org/10.26434/chemrxiv-2024-g54bp **ORCID:** https://orcid.org/0000-0002-7854-8207 Content not peer-reviewed by ChemRxiv. **License:** CC BY-NC-ND 4.0

Investigation of secondary metabolites from plant endophytic fungi has become our interest in recent years, and some structurally and biologically intriguing compounds have been isolated by us.[19] Previously, a strain of *Bipolaris victoriae* S27 derived from *Rubia cordifolia* was selected for chemical investigation, and a total of 45 compounds were obtained, such as antitumor meroterpenoids, [19d] (−)-*N*-hydroxyapiosporamide, [19h] sativene sesquiterpenoids,[20] nonadrides. Notably, *Bipolaris* genus possess more than 32 specialised metabolite clusters encoding core enzymes and cytochrome P450, one of them may be responsible for dimerization.[21] Therefore, further chemical investigation is still necessary for genus *Bipolaris* due to their potent ability to produce novel anti-tumour compounds including dimers.

Here, we aimed to study the chemical diversity of *B. victoriae* S27 with metabolomic method of OSMAC (one strain, many compounds) combining molecular network, screen for new antitumor drugs, and explore novel anti-CRC targets and mechanisms. A total of twelve unprecedented chemical architectures terpene-nonadride heterodimers, bipoterprides A–L (**1**–**12**), and their monomers (**13**–**20**) were isolated from the plant endophytic *B. victoriae* S27. Compounds **1**–**12** represented the first example of terpene-nonadride heterodimers, in which nonadride monomers of **1** and **2** were also the first example of 5/6 bicyclic nonadrides with carbon rearrangements. The pharmacological mechanism by which **2** was investigated with proteomics, bioinformatics, clinical tissue sample, and a series of functional assays. Mechanistically, DCTPP1 was identified as a new target for CRC therapy, and **2** bound to DCTPP1, inhibited its enzymatic activity, and intervened with amino acid metabolic reprogramming, thereby exhibiting potent

https://doi.org/10.26434/chemrxiv-2024-g54bp **ORCID:** https://orcid.org/0000-0002-7854-8207 Content not peer-reviewed by ChemRxiv. **License:** CC BY-NC-ND 4.0

antitumor activity *in vitro* and *in vivo*.

RESULTS AND DISCUSSION

Metabolomics Study of *Bipolaris victoriae* S27 Using the OSMAC and Molecular Network Strategy

To explore the chemical diversity produced by *B. victoriae* S27 depending on culture media, a complete metabolomics study was performed. The fungus was cultured in seventy-six kinds of media (Table S1), and their extracts were screened by HPLC. The results (Figures 1a and S1) indicated that media XXXI, XXXVIII, XLVIII, and LIII showed abundant metabolites with visible differences comparing to that of rice medium studied by us previously.[19d] In addition, chemical profiles comparison was performed by the heatmap generated with hierarchical clustering analysis (Figure 1b), and the cluster exhibited high abundances (red) in medium LIII and low abundances in other media, which revealed that the media LIII had a significant influence on metabolites production with higher differences to rice medium. Above analysis could be assumed that the level of expression of the BGCs was enhanced by the indicated medium.

To further investigate the secondary metabolites produced by the *B. victoriae* S27, molecular networks was applied to establish structural relationships and perform dereplication on the different detected ions. As shown in Figure 1c, the molecular network showed obviously differences in secondary metabolites depending on the culture media. It was important to note that some interesting molecular clusters, consisting of two monomer ions at *m/z* 363 and 331 together with possible dimers at 555, 569, 601, 639, 632, 567, and 733, caught our attentions, which are most abundant

https://doi.org/10.26434/chemrxiv-2024-g54bp **ORCID:** https://orcid.org/0000-0002-7854-8207 Content not peer-reviewed by ChemRxiv. **License:** CC BY-NC-ND 4.0

in medium LIII. Therefore, this medium was considered as most promising fermentation condition, and then the study focused on the indicated cluster with above ions.

Isolation and Structure Elucidation

Twelve unprecedented chemical architectures terpene-nonadride heterodimers, bipoterprides A–L (**1**–**12**), and eight terpene or nonadride monomers (**13**–**20**) including three new ones bipolodrides A (**13**) and B (**14**) and bipolenin O (**18**), were isolated from the plant endophytic *B. victoriae* S27 derived from the stem of *R. cordifolia* (Figure 2). Their structures with full configurations were determined by comprehensive spectroscopic analysis, calculations, chemical reactions, and X-ray crystals.

Bipoterpride A (**1**) was obtained as colourless needle crystals, whose molecular formula was established as $C_{34}H_{50}O_9$ (10 degrees of unsaturation) based on HRESIMS ($[M+Na]^+$, 625.33502, calcd 625.33470) and supported by ^1H and ^{13}C NMR spectroscopic data (Tables S2 and S5). The IR spectrum showed absorption bands at 3363, 2957, 2928, 1730, 1712, 1463, 1251,1216, 1024 and 890 cm^{-1}, which indicated the presence of hydroxyl, carbonyl, and double bond functional groups. The UV spectrum exhibited maximum absorption bands at λ_{max} 202 nm, suggesting that **1** contained a conjugated double bond system. The 1D NMR spectra and HSQC spectrum of **1** revealed the presence of six sp^3 methyl proton signals at δ_H 0.74, 0.83, 3.35, 0.92, 0.80, and 0.96, and their corresponding carbons signals at δ_C 14.6 (CH_3-14), 13.3 (CH_3-17), 50.8 (OCH_3-19), 21.2 (CH_3-10'), 20.7 (CH_3-11'), and 20.4 (CH_3-13'); nine sp^3 methylene proton signals at δ_H 2.87 and 2.68, 2.73 and 1.54, 1.11 and 1.05, 2.04 and

https://doi.org/10.26434/chemrxiv-2024-g54bp **ORCID:** https://orcid.org/0000-0002-7854-8207 Content not peer-reviewed by ChemRxiv. **License:** CC BY-NC-ND 4.0

1.40, 1.55 and 1.05, 1.46 and 1.28, 1.63 and 0.98, 3.94 and 3.69, 3.46 and 3.09 and their corresponding carbons at δ_C 28.6 (CH_2-4), 37.8 (CH_2-7), 23.7 (CH_2-15), 31.8 (CH_2-16), 29.9 (CH_2-18), 42.0 (CH_2-2'), 24.7 (CH_2-3'), 65.9 (CH_2-14') and 65.2 (CH_2-15'); one sp^2 methylene proton signals at δ_H 4.98 and 4.78, and its corresponding carbons at δ_C 105.3 (CH_2-12'); eight sp^3 methine proton signals at δ_H 2.92, 2.05, 1.52, 1.08, 2.22, 2.39, 1.60, and 1.29, and their corresponding carbons at δ_C 43.1 (CH-5), 44.3 (CH-8), 57.9 (CH-9), 48.9 (CH-4'), 39.5 (CH-5'), 45.7 (CH-6'), 53.8 (CH-8'), and 30.1 (CH-9'); one sp^2 methine proton signals at δ_H 7.03, and its corresponding carbons at δ_C 138.7 (CH-3). In addition, the ^{13}C NMR spectrum of **1** revealed three sp^3 quaternary carbon: C-1 (δ_C 61.4), C-6 (δ_C 55.4), and C-1' (δ_C 47.4), and six sp^2 hybridized carbons including two carboxyl carbon [COOH-11 (δ_C 167.2) and COOH-13 (δ_C 173.8)], two ester carbonyls [COO-10 (δ_C 171.1) and COO-12 (δ_C 172.4)], and two olefinic carbons [C-2 (δ_C 131.2) and C-7' (δ_C 158.3)]. Preliminary analysis on the NMR data, two moieties of nonadride (unit A) and sativene sesquiterpenoid (unit B) were detected by comparison of the data with literature.[22]

For unit A, as shown in Figure S2, the $^1H-^1H$ COSY correlations led to the identification of two spin systems, segments I (C3−C5) and II (C7−C9, C17−C18−C8, and C14−C16−C9), the HMBC correlations from H-9 to C-1 and C-2, H-8 and H-3 to C-1, H-7 to C-6 and C-5, H-4 to C-2 and C-6, and H-16 to C-1 revealed the nine-membered ring as constructed by C-1, C-2, C-3, C-4, C-5, C-6, C-7, C-8 and C-9. In addition, the key HMBC correlations from H-7 and H-9 to C-1 and C-6 suggested the connection between C-1 and C-6, reducing the nine-membered ring into five- and six-

https://doi.org/10.26434/chemrxiv-2024-g54bp ORCID: https://orcid.org/0000-0002-7854-8207 Content not peer-reviewed by ChemRxiv. License: CC BY-NC-ND 4.0

membered rings. Moreover, the HMBC correlations from H-3 to C-11, H-4 to C-12, H-7 to C-13, and H-9 to C-10 as well as the chemical shifts showed that the four carbonyl groups were located at C-10, C-11, C-12, and C-13, respectively. The HMBC correlation from H-19 to C-10 and the chemical shifts of C-19 implied the presence of a methoxy group at C-10. According to the MS data and chemical shift values, the remaining three carbons (C-11, C-12, and C-13) were attributed to two acid groups and one ester carbonyl. To our knowledges, unit A represented the first example of 5/6-fused core skeleton nonadride with carbon rearrangement.

For unit B, a long spin system was obtained by analysis of the ^{1}H–^{1}H COSY spectrum (Figure S2). In the HMBC spectrum, a singlet for H-13' showed correlations to C-2', C-7', C-8', and C-1', which was very important for the establishment of three C–C bonds of C-2', C-7', and C-8' with C-1', respectively. In addition, the key HMBC correlations from H-12' to C-1', C-6' and C-7', and from H-5' to C-1' and C-7' suggested the connection between C-1', C-7' and C-6'. This information and ^{1}H–^{1}H COSY correlations (H-2'/H-3'/H-4'/H-5'/H-6') revealed a seven-membered ring constructed by C-1', C-2', C-3', C-4', C-5', C-6', and C-7'. Furthermore, the connection between C-8' and C-5' has been proved by the ^{1}H–^{1}H COSY correlation (H-5'/H-8'). Therefore, a bridged carbon bond of C-1'–C-8'–C-5' was established, which reduced the seven-membered ring into six- and five-membered rings. These data and ^{1}H–^{1}H COSY correlations (H-4'/H-9'/H-11', H-9'/H-10', H-6'/H-15', and H-8'/H-14') and HMBC correlations (from H-14' to C-1', from H-15' to C-7') suggested that unit B was a sativene sesquiterpenoid related to the dihydroprehelminthosporol (**15**),[22] which was

https://doi.org/10.26434/chemrxiv-2024-g54bp **ORCID:** https://orcid.org/0000-0002-7854-8207 Content not peer-reviewed by ChemRxiv. **License:** CC BY-NC-ND 4.0

also isolated in this study.

Finally, the units A and B were connected by an ester bond like taxol, which was confirmed by HMBC from H-14' to C-12, as well as analysis of the MS data. Therefore, the planar structure of **1** was established (Figure 2).

Compound **1** contains ten stereocenters at C-1, C-5, C-6, C-8, C-9, C-1', C-4', C-5', C-6' and C-8', and its relative configurations were determined by the ROESY correlations (H-8/H-16, H-5/H-7b/H-9/H-18, H-5'/H-14'/H-13'/H-15' and H-8'/H-6'/H-9') and calculated ^{13}C NMR data (Figures S3 and S4) as 1*R**, 5*S**, 6*S**, 8*R**, 9*S**, 1′*R**, 4′*R**, 5′*R**, 6′*R**, and 8′*S**. Moreover, the absolute configuration of **1** was determined by X-ray crystal diffraction (CCDC 2233210, Figure 3) with flack parameter of 0.34 (6), and calculated ECD (Figure S5) as 1*R*, 5*S*, 6*S*, 8*R*, 9*S*, 1′*R*, 4′*R*, 5′*R*, 6′*R*, and 8′*S*.

Detailed structure elucidation of **2**–**20** was depicted in the Supporting Information. Compounds **1**–**12** represented the first example of terpene-nonadride heterodimers, in which nonadride monomers of **1** and **2** are also first example of 5/6 bicyclic nonadrides. In order to further confirm the established structures, chemical reaction products of some terpene-nonadride heterodimers were detected with the UPLC-MS/MS MRM method. The results indicated that **3**, **5**, **6**, **8**, **9**, **11** and **12**, whose monomers are identical with **13**, **15**, and **17**–**20** (Figure S7). Besides, incubation of **3**, **5**, **6**, **8**, **9**, **11** and **12** in mildly acidic buffers failed to break the ester linkage (Figure S8). Simultaneously, incubation of monomers also failed to lead conversion of heterodimers (Figure S9). These results indicated that these terpene-nonadride heterodimers are not artificial products.

https://doi.org/10.26434/chemrxiv-2024-g54bp **ORCID:** https://orcid.org/0000-0002-7854-8207 Content not peer-reviewed by ChemRxiv. **License:** CC BY-NC-ND 4.0

Discovery of 2 as Potent Inhibitors of CRC *in vitro* and *in vivo*

All obtained compounds were evaluated for their cytotoxicity on five human CRC cell lines. As shown in Figures 4a and 4b, and Table S8, compound **2** displayed the most pronounced activities on all tested cell lines, which was comparable to the first-line drug 5-FU and superior to cisplatin. The heterodimers exhibited an obviously important impact on their anti-tumor activity (Table S8). Besides, comparison of anti-tumor activity of heterodimers revealed that C1–C6 bond and configuration of 5*R* may also be important for their activities. To investigate the effects of combined treatment with monomers on anti-tumor activity, compounds "**13**+**15**", "**13**+**17**", and "**13**+**18**" were selected and grouped to detected their cytotoxicity, and the results showed that these make no positive difference for cytotoxicity of monomers. Considering cytotoxicity and obtained monomers, we also detected **6** in HCT116 cells after treatment at **3**, **6**, **12**, and **24** h. As expected, only **6** could be detected, and its monomers could not be detected, which indicated that **6** showed anti-tumor activity with the type of heterodimers (Figures 4c and S15).

Based on the cytotoxic data (Table S8) and universalities of the chosen CRC cell lines in the preclinical study, we chose HCT116 cell to investigate the potential antitumor mechanism of **2**. Clonogenic assay was performed to evaluate the effects on cell proliferation, and the results showed that **2** could dose-dependently reduce the clonogenicity of HCT116 cells (Figure 4d). Besides, we also performed cell cycle assay using flow cytometer and detected the expression of cell cycle related proteins with western blotting. The results showed that **2** could obviously accumulate the cells in

https://doi.org/10.26434/chemrxiv-2024-g54bp **ORCID:** https://orcid.org/0000-0002-7854-8207 Content not peer-reviewed by ChemRxiv. **License:** CC BY-NC-ND 4.0

G_0/G_1 phase and decrease the cells in G_2/M phase (Figure 4e), and reduce the expressions of Cdc25c, CDK1, CDK2, CDK4, Cyclin B, and Cyclin D (Figure 4f). Moreover, compound **2** could also induce apoptotic and autophagic CRC cell death, details see Supporting Information and Figures S12 and S13. To determine the *in vivo* antitumor efficacy of **2**, CRC xenograft mouse models were established. As shown in Figures 4g-i, compound **2** dose-dependently suppressed the growth of CRC xenograft tumors, with obvious reduction in the tumor weight and volume as compared to the vehicle group. Furthermore, the immunohistochemistry analysis for apoptosis- and autophagy-associated marker proteins in the tumor tissues showed that **2** promoted the expression of cleaved caspase-3, cleaved PARP and LC3A/B, while it reduced the expression of p62 (Figure S10). Meanwhile, there was no significant difference in the body weight, hematoxylin-eosin staining, and levels of some representative serum markers for liver damage between the vehicle group and the **2**-treated groups (Figure S11). Taken together, these results demonstrated that **2** exhibited potent cytotoxicity, induced apoptosis and autophagy in CRC tumor cells, eventually leading to tumor necrosis *in vivo* without obviously toxicity in the effective doses.

High DCTPP1 Expression in CRC is Correlated with Poor Patient Survival

The prominent inhibitory effects of **2** on CRC *in vitro* and *in vivo* prompted us to identify its possible targets. To investigate the molecular mechanisms of **2** exerting anticancer bioactivity, the drug affinity responsive target stability (DARTS) technology and mass spectrometry analysis were performed (Figure 5a), and 14 proteins were identified as potential targets of **2** with high coverage and significant differences (Figure

https://doi.org/10.26434/chemrxiv-2024-g54bp **ORCID:** https://orcid.org/0000-0002-7854-8207 Content not peer-reviewed by ChemRxiv. **License:** CC BY-NC-ND 4.0

S16). Among the candidate proteins, the top six proteins of were listed (Figure 5b), and the coverage of DCTPP1 is much larger than others. Therefore, we considered DCTPP1 may be the target of **2**, and further investigated the uncharted relations of DCTPP1 proteins with CRC and **2**. It has been reported that DCTPP1 is highly expressed in lung, stomach, prostate, and breast cancers (Figure 5c), but the expression of DCTPP1 protein in colorectal cancer remain unclear. The DCTPP1 expression in CRC was evaluated by TCGA data, and the results showed that DCTPP1 is highly expressed in CRC. Moreover, immunohistochemistry (IHC) assays were also performed in clinical CRC tissues and the tissue microarray containing adjacent- and tumour-human CRC samples. As shown in Figures 5e, 5f, and S17, significant upregulation of expression had a significantly shorter survival ($p < 0.05$, Figure 5g), which were confirmed by TCGA dataset and bioinformatics analysis (Supporting information).

Compound 2 Exhibit Anti-Colorectal Cancer Activity Through Directly Targeting DCTPP1 to Intervene with Metabolic Reprogramming

In order to further verify the cellular interaction between **2** and DCTPP1, surface plasmon resonance (SPR) analysis was performed, and the results showed that **2** could bind to the DCTPP1 protein with a higher affinity (Kd = 3.8 μM) relative to representative monomers **13** and **15** (Figure 6a). Then compound binding was further validated through isothermal titration calorimetry (ITC) experiments, revealing Kd values of 4.69 μM (Figures 6b and 6c). Furthermore, a DARTS assay was performed. As expected, the DCTPP1 protein becomes protease-resistant in the presence of **2** (Figure 6d), indicating that **2** directly interact with DCTPP1 in CRC cell lysates. A

https://doi.org/10.26434/chemrxiv-2024-g54bp **ORCID:** https://orcid.org/0000-0002-7854-8207 Content not peer-reviewed by ChemRxiv. **License:** CC BY-NC-ND 4.0

cellular thermal shift assay (CETSA) approach was also used to assess their binding affinity, which indicated that **2** could stabilize DCTPP1 at higher temperatures compared with DMSO treatment (Figure 6e). These data strongly suggest that DCTPP1 is a specific target of **2**. To further identify the binding site for **2** in DCTPP1, we conducted molecular docking simulation to predict the interaction of **2** with the DCTPP1 protein (Figure 6f). Results showed that **2** may bind to the DCTPP1 protein by contacts with the amino acid residues, including Phe (25), Ser (26), Glu (28), Pro (29), Thr (30), Leu (31), Ile(34), Glu (93), Ser (97), Leu (100). More importantly, knockdown of DCTPP1 substantially decreased the inhibitory effect of **2** on HCT116 cell proliferation, inversely, overexpression of DCTPP1 increased the sensitive of HCT116 cells to **2** (Figures 6g and 6h).

Enzyme activity of DCTPP1 could reflect the intensity of DCTPP1 inhibition by compounds. Therefore, ELSIA assay was performed, and the results indicated that **2** inhibits the enzyme activity of DCTPP1 with an IC_{50} value of 5.08 μM (Figure 6i). Nucleotide metabolism could relate amino acid for immune cell activation and anti-tumor effects in the tumor microenvironment. The abnormal changes of amino acid metabolism are closely related to tumor development and immunity. As an important protease in nucleotide metabolism, knockdown of DCTPP1 will results in amino acid metabolic reprogramming, for example, the down-regulation of arginine, glutamine, and proline, thereby suppressing tumor growth.[15] Therefore, we established amino acid metabolomics detection method based on UPLC MS/MS MRM technology, and found that **2** (10 μM) can induce amino acid reprogramming and reduce the content of amino

https://doi.org/10.26434/chemrxiv-2024-g54bp **ORCID:** https://orcid.org/0000-0002-7854-8207 Content not peer-reviewed by ChemRxiv. **License:** CC BY-NC-ND 4.0

acids in HCT116 cells (Figure 6j), especially for arginine, glutamine, and proline (Figure 6k). Many studies have shown that metabolic reprogramming of tumor cells plays an important role in ROS production, antioxidant system activation and maintenance of REDOX homeostasis, therefore, the production of intracellular ROS regulated by **2** and its positive effects on some tumor-related signaling pathways were investigated. The results showed that **2** could increase the ROS generation and inhibit the NF-κB and Akt/mTOR/P70S6K signaling in HCT116 cells (Supporting information, Figure S14). These results indicated that **2** suppresses colorectal cancer via targeting DCTPP1 to intervene with acid metabolic reprogramming.

Evaluation of Pharmacokinetics of 2 in Sprague-Dawley Rats

Bioactive compounds with good pharmacokinetic properties can greatly contribute to drug development, then we also performed pharmacokinetic experiments of **2** in Sprague-Dawley rats (Supporting information, Table S9). Compound **2** was administered (*i.v.* and *i.p.*) in mice at a dose of 20 mg/kg bodyweight. The C_{max} value and half time of **2** was 15776 ± 3750 ng/mL (*i.v.*) for 6 min, and 5050 ± 341 ng/mL (*i.p.*) for 264 min. Moreover, plasma clearance (CL) was 0.032 ± 0.004 (*i.v.*) and 0.004 ± 0.001 (*i.p.*) L/min/kg, respectively. The $t_{1/2}$ value of 5-FU in mice is 1.36 h (*i.p.*) according to the previous report, which is shorter than that of **2**. Therefore, these pharmacokinetic parameters were within an acceptable range, and indicated that **2** with good pharmacokinetic characteristics was a potential drug candidate in CRC.

CONCLUSION

https://doi.org/10.26434/chemrxiv-2024-g54bp **ORCID:** https://orcid.org/0000-0002-7854-8207 Content not peer-reviewed by ChemRxiv. **License:** CC BY-NC-ND 4.0

Colorectal cancer (CRC) is the third most common cancer globally with a high rate of 10 % in new cancer cases, which is the second deadliest cancer in the world. Identification of new effective drug targets of CRC and exploration of bioactive small-molecules are clinically urgent and the hot spots in tumor therapy. In the current study, twelve unprecedented chemical architectures terpene-nonadride heterodimers bipoterprides A–L (**1**–**12**) and eight their monomers (**13**–**20**) were isolated from the plant endophytic *Bipolaris victoriae* S27 derived from the stem of *Rubia cordifolia*. Compounds **1**–**12** represented the first example of terpene-nonadride heterodimers, in which nonadride monomers of **1** and **2** are also first example of a 5/6 bicyclic nonadrides with carbon rearrangements. All obtained compounds were evaluated for their cytotoxicity against five human colorectal cancer cell lines (HCT116, SW480, HT29, RKO, and SW620), and the results showed that nine compounds (**2**–**4**, **6**, and **8**–**12**) exhibited cytotoxicity ranging from 3.37 to 38.7 μM. The meaningful SARs could be summarized as follows: (i) the heterodimers were essential for their anti-CRC activity; (ii) the C-1–C-6 bond was favorable for their anti-CRC activity; and (iii) the configuration of 5*R* also had effect on their anti-CRC activity. Moreover, compound **2** showed promising anti-CRC efficacy in *vivo* and with an acceptable pharmacokinetic data. Notably, we did not observe obvious toxic effects of the **2** *in vivo* throughout the experiments. Besides, compound **2** could also induce apoptotic and autophagic cell death. To investigate the molecular mechanisms of **2** exerting anticancer bioactivity, the DARTS technology and mass spectrometry analysis were performed. Then, a series of functional assays, clinical tissues sample data, and bioinformatics analysis were used

https://doi.org/10.26434/chemrxiv-2024-g54bp **ORCID:** https://orcid.org/0000-0002-7854-8207 Content not peer-reviewed by ChemRxiv. **License:** CC BY-NC-ND 4.0

to demonstrate that **2** binds to DCTPP1, inhibits its enzymatic activity, and intervenes with amino acid metabolic reprogramming. All in all, these results showed that DCTPP1 is a novel potential biomarker and therapeutic target in CRC, and **2** is the first natural anti-CRC drug candidate targeting DCTPP1, providing a promising template for developing novel anti-CRC targets and effective agents in the future.

SUPPORTING INFORMATION

The Supporting Information is available free of charge on the ACS Publications website. Detailed structural elucidation and NMR data of **1**−**20**; molecular docking of **2**; experimental section; MS, UV, IR, and NMR spectra of **1**−**14** and **18**; calculations of **1**−**12**; crystallographic data for **1**, **3**, and **12** (CIF**).**

ACKNOWLEDGEMENTS

This work was supported by the National Natural Science Foundation of China (32070387, 32300338, 32070356, 82102737), the Fundamental Research Funds for the Central Universities (2632023GR05), the "Double First Class" University Project of China Pharmaceutical University (CPUQNJC22_05), and the Jiangsu Excellent Postdoctoral Program (2023ZB126). We thank Dr. Hui-Min Xu of the Public Laboratory Platform at China Pharmaceutical University for assistance with NMR techniques.

https://doi.org/10.26434/chemrxiv-2024-g54bp **ORCID:** https://orcid.org/0000-0002-7854-8207 Content not peer-reviewed by ChemRxiv. **License:** CC BY-NC-ND 4.0

REFERENCES

[1] (a) R. L. Siegel, K. D. Miller, N. S. Wagle, A. Jemal, *CA Cancer J. Clin.* **2023**, *73*, 17–48. (b) H. Sung, J. Ferlay, R. L. Siegel, M. Laversanne, I. Soerjomataram, A. Jemal, F. Bray, *CA Cancer J. Clin.* **2021**, *71*, 209–249.

[2] F. M. Brodsky, *Pharm. Res*. **1988**, *5*, 1–9.

[3] Y. H. Xie, Y. X. Chen, J. Y. Fang, *Signal Transduct Target Ther.* **2020**, *5*, 22–23.

[4] R. Yaeger, J. Weiss, M. S. Pelster, A. I. Spira, M. Barve, S. I. Ou, T. A. Leal, T. S. BekaiaiSaab, C. P. Paweletz, G. A. Heavey, J. G. Christensen, K. Velastegui, T. Kheoh, H. DerTorossian, S. J. Klempner, *N Engl J Med.* **2023**, *388*, 44–54.

[5] C. Bailly, *Pharmacol. Res*. **2019**, *148*, 104398–104400.

[6] (a) H. Gad, T. Koolmeister, A. S. Jemth, S. Eshtad, S. A. Jacques, C. E. Strom, L. M. Svensson, N. Schultz, T. Lundback, B. O. Einarsdottir, A. Saleh, C. Gokturk, P. Baranczewski, R. Svensson, R. P. Berntsson, R. Gustafsson, K. Stromberg, K. Sanjiv, M. C. Jacques-Cordonnier, M. Desroses, A. L. Gustavsson, R. Olofsson, F. Johansson, E. J. Homan, O. Loseva, L. Brautigam, L. Johansson, A. Hoglund, A. Hagenkort, T. Pham, M. Altun, F. Z. Gaugaz, S. Vikingsson, B. Evers, M. Henriksson, K. S. Vallin, O. A. Wallner, L. G. Hammarstrom, E. Wiita, I. Almlof, C. Kalderen, H. Axelsson, T. Djureinovic, J. C. Puigvert, M. Haggblad, F. Jeppsson, U. Martens, C. Lundin, B. Lundgren, I. Granelli, A. J. Jensen, P. Artursson, J. A. Nilsson, P. Stenmark, M. Scobie, U. W. Berglund, T. Helleday, *Nature.* **2014**, *508*, 215−219. (b) C. E. Requena, G. Perez-Moreno, A. Horvath, B.

https://doi.org/10.26434/chemrxiv-2024-g54bp **ORCID:** https://orcid.org/0000-0002-7854-8207 Content not peer-reviewed by ChemRxiv. **License:** CC BY-NC-ND 4.0

G. Vertessy, L. M. Ruiz-Perez, D. Gonzalez-Pacanowska, A. E. Vidal, *Biochem. J.* **2016**, *473*, 2635−2643.

[7] (a) Q. Huang, C. Tan, C. Zheng, H. Meng, Z. Wang, G. Q. Lin, W. Zhang, B. Chen, Q. L. He, *Phytomedicine*. **2023**, *119*, 154972−154973. (b) F. F. Song, L. L. Xia, P. Ji, Y. B. Tang, Z. M. Huang, L. Zhu, J. Zhang, J. Q. Wang, G. P. Zhao, H. L. Ge, Y. Zhang, Y. Wang, *Oncogenesis*. **2015**, *15*, 1038−1042. (c) S. Llona-Minguez, M. Haggblad, U. Martens, A. Throup, O. Loseva, A. S. Jemth, B. Lundgren, M. Scobie, T. Helleday, *Bioorg. Med. Chem. Lett.* **2017**, *27*, 3897−3904. (d) S. Llona-Minguez, M. Haggblad, U. Martens, L. Johansson, K. Sigmundsson, T. Lundback, O. Loseva, A. S. Jemth, B. Lundgren, A. J. Jensen, M. Scobie, T. Helleday, *Bioorg. Med. Chem. Lett.* **2017**, *27*, 3219-3225.

[8] J. Lu, W. Dong, H. He, Z. Han, Y. Zhuo, R. Mo, Y. Liang, J. Zhu, R. Li, H. Qu, L. Zhang, S. Wang, R. Ma, Z. Jia, W. Zhong, *Int J Biol Macromol.* **2018**, *118*, 599-609.

[9] A. Friese, S. Kapoor, T. Schneidewind, S. R. Vidadala, J. Sardana, A. Brause, T. Forster, M. Bischoff, J. Wagner, P. Janning, S. Ziegler, H. Waldmann, *Angew. Chem. Int. Ed.* **2019**, *58*, 13009–13012.

[10] M. Butler, L. T. Vandermeer, F. N. Vanleeuwen, *Trends. Endocrinol. Metab.* **2021**, *32*, 367-81.

[11] (a) T. W. Corson, H. Cavga, N. Aberle, C. M. Crews, *Chembiochem.* **2011**, *12*, 1767–1773. (b) T. Kambe, B. E. Correia, M. J. Niphakis, B. F. Cravatt, *J. Am. Chem. Soc.* **2014**, *136*, 10777−10782. (c) M. S. Llona, A. Hoglund, S. A. Jacques,

https://doi.org/10.26434/chemrxiv-2024-g54bp **ORCID:** https://orcid.org/0000-0002-7854-8207 Content not peer-reviewed by ChemRxiv. **License:** CC BY-NC-ND 4.0

L. Johansson, J. M. Calderon Montano, M. Claesson, O. Loseva, N. C. K. Valerie, T. Lundback, J. Piedrafita, G. Maga, E. Crespan, L. Meijer, E. B. Morón, P. Baranczewski, A. L. Hagbjork, R. Svensson, E. Wiita, I. Almlof, T. Visnes, F. Jeppsson, K. Sigmundsson, A. J. Jensen, P. Artursson, A. S. Jemth, P. Stenmark, U. W. Berglund, M. Scobie, T. Helleday, *J. Med. Chem.* **2016**, *59*, 1140−1148. (d) S. Llona-Minguez, A. Hoglund, E. Wiita, I. Almlof, A. Mateus, J. M. Calderon-Montano, C. Cazares-Korner, E. Homan, O. Loseva, P. Baranczewski, A. S. Jemth, M. Haggblad, U. Martens, B. Lundgren, P. Artursson, T. Lundback, J. A. Jenmalm, B. U. Warpman, M. Scobie, T. Helleday, *J. Med. Chem.* **2017**, *60*, 2148−2154. (e) S. Llona-Minguez, A. Hoglund, A. Ghassemian, M. Desroses, J. M. Calderon-Montano, E. Burgos-Moron, N. C. K. Valerie, E. Wiita, I. Almlof, T. Koolmeister, A. Mateus, C. Cazares-Korner, K. Sanjiv, E. Homan, O. Loseva, P. Baranczewski, M. Darabi, A. Mehdizadeh, S. Fayezi, A. S. Jemth, U. Warpman-Berglund, K. Sigmundsson, T. Lundback, A. Jenmalm-Jensen, P. Artursson, M. Scobie, T. Helleday, *J. Med. Chem.* **2017**, *60*, 4279−4292.

[12] (a) D. J. Newman, C. M. Cragg, *J. Nat. Prod.* **2020**, *83*, 770–803. (b) H. W. Zhang, Y. C. Song, R. X. Tan, *Nat. Prod. Rep.* **2006**, *23*, 753–771.

[13] T. R. Govindachari, P. C. Parthasarathy, *Tetrahedron* **1971**, *27*, 1013-1026.

[14] Z. R. Cui, Y. Wang, J. Li, J. Chi, P. Zhang, L. Y. Kong, J. Luo, *Org. Lett.* **2022**, *24*, 9107–9111.

[15] W. S. Li, J. Wu, J. Li, T. Satyanandamurty, L. Shen, G. Bringmann, *Org. lett.* **2017**, *19*, 182-185.

https://doi.org/10.26434/chemrxiv-2024-g54bp **ORCID:** https://orcid.org/0000-0002-7854-8207 Content not peer-reviewed by ChemRxiv. **License:** CC BY-NC-ND 4.0

[16] (a) N. Tajuddeen, F. R. Van-Heerden, *Malar. J.* **2019**, *18*, 404-406. (b) R. A. Fernandes, P. H. Patil, D. A. Chaudhari, *Eur. J. Org. Chem.* **2016**, *12*, 5778–5798. (c) H. Hussain, A. Al-Harrasi, I. Green, Z. Hassan, I. Ahmed, *Stud. Nat. Prod. Chem.* **2015**, *46*, 447–517.

[17] (a) L. F. Tietze, B. D. Hubertus, S. Chandrasekhar, *Angew. Chem. Int. Ed.* **2003**, *42*, 3996–4028. (b) C. Reiter, A. C. Karagoz, T. Frohlich, V. Klein, M. Zeino, K. Viertel, J. Held, B. Mordmüller, S. E. Oztürk, H. Anıl, T. Efferth, S. B. Tsogoeva, *Eur. J. Med. Chem.* **2014**, *75*, 403–412.

[18] (a) P. R. Cao, M. Li, J. S. Zhang, Y. L. Zheng, J. Chen, Y. Q. Zhao, X. D. Qi, P. H. Zhu, Y. C. Gu, L. Y. Kong, M. H. Yang, *Org. Lett.* **2022**, *24*, 6789–6793. (b) C. Sun, Q. Liu, M. Shah, Q. Che, G. J. Zhang, T. J. Zhu, J. F. Zhou, X. Z. Rong, D. H. Li, *Org. Lett.* **2022**, *24*, 3993–3997.

[19] (a) L. Feng, A. X. Zhang, R. R. Shang, X. J. Wang, N. H. Tan, Z. Wang, *J. Org. Chem.* **2022**, *87*, 14058–14067. (b) X. Li, Y. X. Gong, L. Feng, X. J. Wang, J. W. Wang, A. X. Zhang, N. H. Tan, Z. Wang, *Phytochemistry* **2022**, *207*, 113579–113582. (c). Feng, J. Wang, S. Liu, X. J. Zhang, Q. R. Bi, Y. Y. Hu, Z. Wang, N. H. Tan, *J. Nat. Prod.* **2019**, *82*, 1434–1441. (d) L. Feng, X. J. Wang, L. Li, A. X. Zhang, R. R. Shang, N. H. Tan, Z. Wang, *Phytochemistry* **2022**, *200*, 113180–113182. (e) L. Feng, J. Han, J. Wang, A. X. Zhang, Y. Y. Miao, N. H. Tan, Z. Wang, *Phytochemistry* **2020**, *179*, 112505–112507. (f) L. Feng, A. X. Zhang, X. J. Zhang, Z. Wang, N. H. Tan, *Lett. Appl. Microbiol.* **2021**, *73*, 759–769. (g) A. X. Zhang, L. Feng, J. Wang, N. H. Tan, Z. Wang, *J. Asian. Nat. Prod. Res.* **2022**, *8*,

https://doi.org/10.26434/chemrxiv-2024-g54bp **ORCID:** https://orcid.org/0000-0002-7854-8207 Content not peer-reviewed by ChemRxiv. **License:** CC BY-NC-ND 4.0

769–776. (h) L. Feng, R. R. Shang, X. J. Wang, L. Li, X. Li, Y. X. Gong, L. Y. Shi, J. W. Wang, Z. Y. Qian, N. H. Tan, Z. Wang, *J. Nat. Prod.* **2023**, *86*, 1449–1462. (i) X. J. Wang, Z. Wang, J. Han, S. H. Su, Y. X. Gong, Y. Zhang, N.H. Tan, J. Wang, L. Feng, *J. Agr. Food Chem.* **2024**, DOI: 10.1021/acs.jafc.3c05815.

[20] Y. Y. Li, X. M. Tan, J. Yang, L. P. Guo, G. Ding, *J. Agric. Food Chem.* **2020**, *68*, 9827–9838.

[21] (a) Y. Wang, H. Kang, J. Yao, Y. F. Wang, H. X. Kang, J. A. Yao, Z. Q. Li, X. Y. Xia, S. Q. Zhou, W. D. Liu, *Phytopathology* **2022**, *112*, 1386–1390. (b) X. Wei, X. Chen, L. Chen, D. X. Yan, W. G. Wang, Y. D. Matsuda, *J. Nat. Prod.* **2021**, *84*, 1544–1549. (c) A. Ishihara, R. Kumeda, N. Hayashi, Y. Yagi, N. Sakaguchi, Y. Kokubo, N. Ube, S. Tebayashi, K Ueno, *Biosci. Biotech. Bioch.* **2017**, *81*, 1090–1098. (d) J. Arunpanichlert, V. Rukachaisirikul, K. Tadpetch, S. Phongpaichit, N. Hutadilok-Towatana, O. Supaphon, J. Sakayaroj, *Phytochemistry Lett.* **2012**, *5*, 604–608.

[22] L. M. Pena-Rodriguez, N. A. Armingeon, W. S. Chilton, *J. Nat. Prod.* **1988**, *51*, 821–828.

https://doi.org/10.26434/chemrxiv-2024-g54bp **ORCID:** https://orcid.org/0000-0002-7854-8207 Content not peer-reviewed by ChemRxiv. **License:** CC BY-NC-ND 4.0

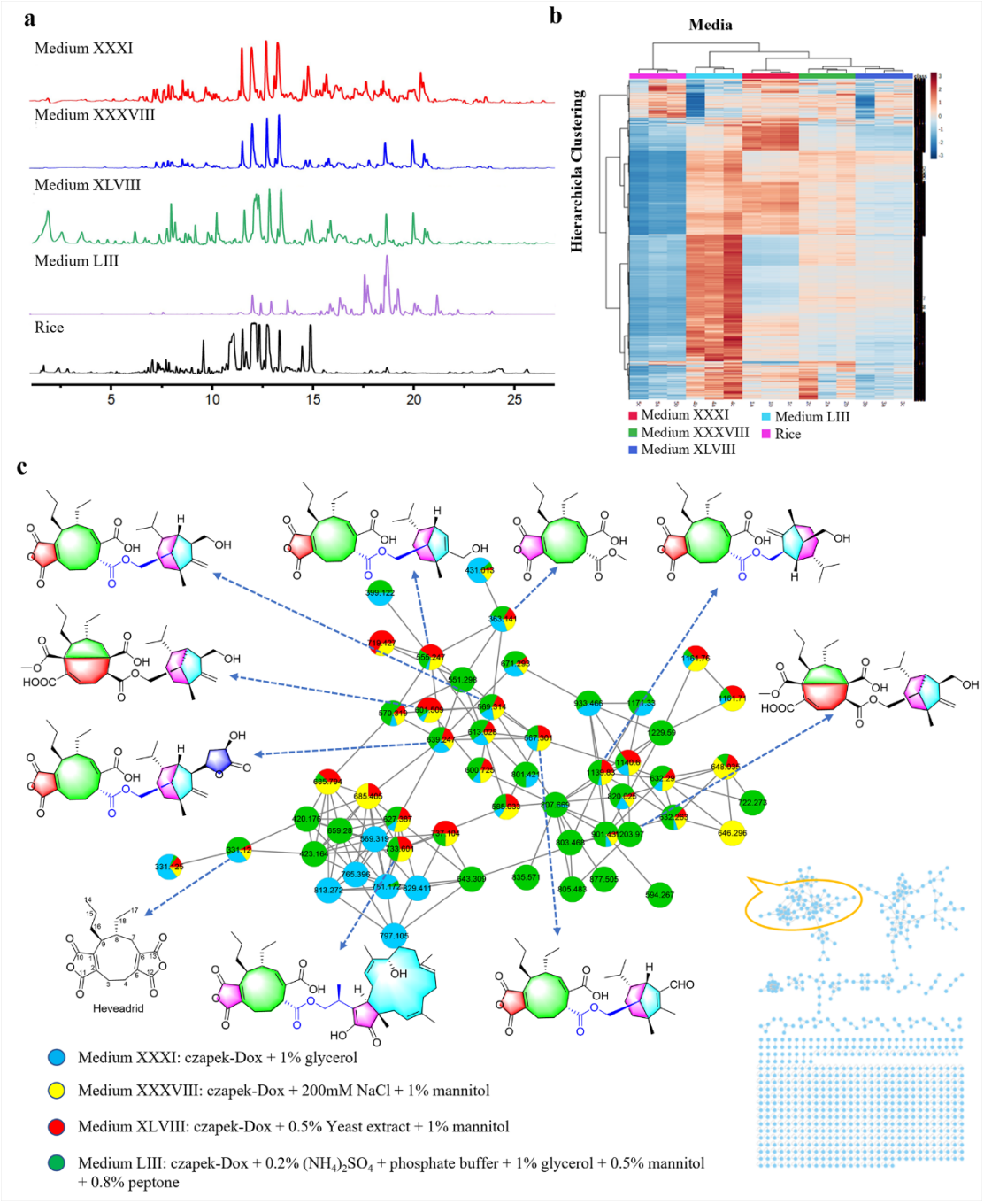

Figure 1. Metabolomic study of the *Bipolaris victoriae* S27

https://doi.org/10.26434/chemrxiv-2024-g54bp **ORCID:** https://orcid.org/0000-0002-7854-8207 Content not peer-reviewed by ChemRxiv. **License:** CC BY-NC-ND 4.0

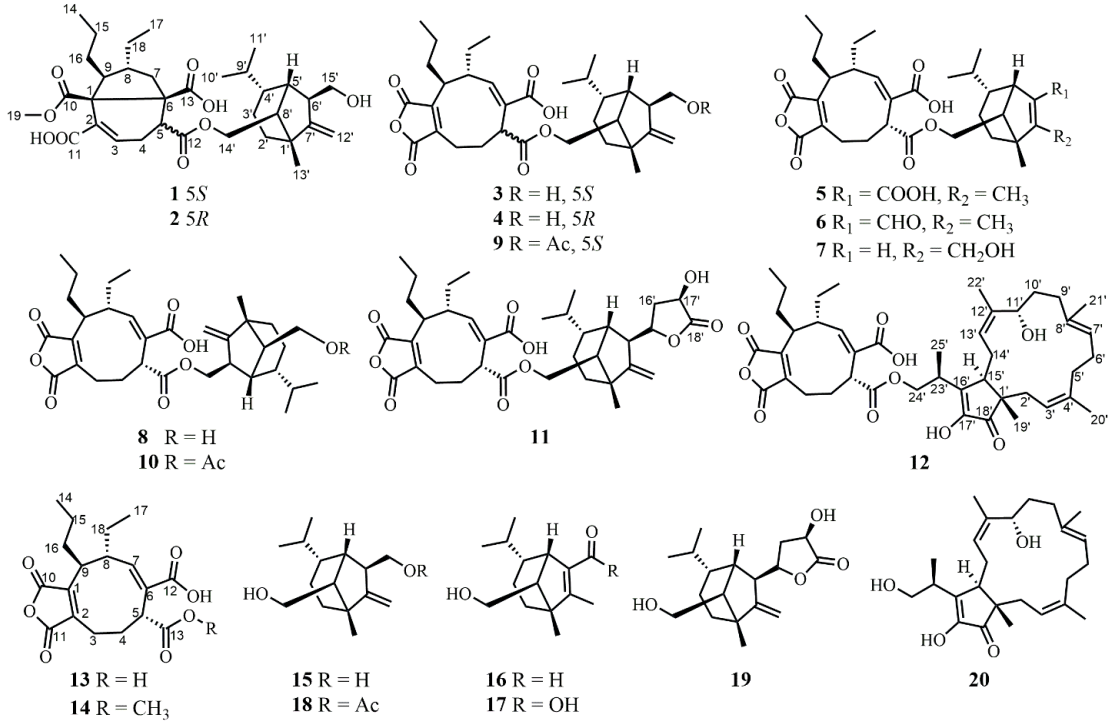

464

465 **Figure 2.** Chemical structures of **1**−**20**

466

https://doi.org/10.26434/chemrxiv-2024-g54bp **ORCID:** https://orcid.org/0000-0002-7854-8207 Content not peer-reviewed by ChemRxiv. **License:** CC BY-NC-ND 4.0

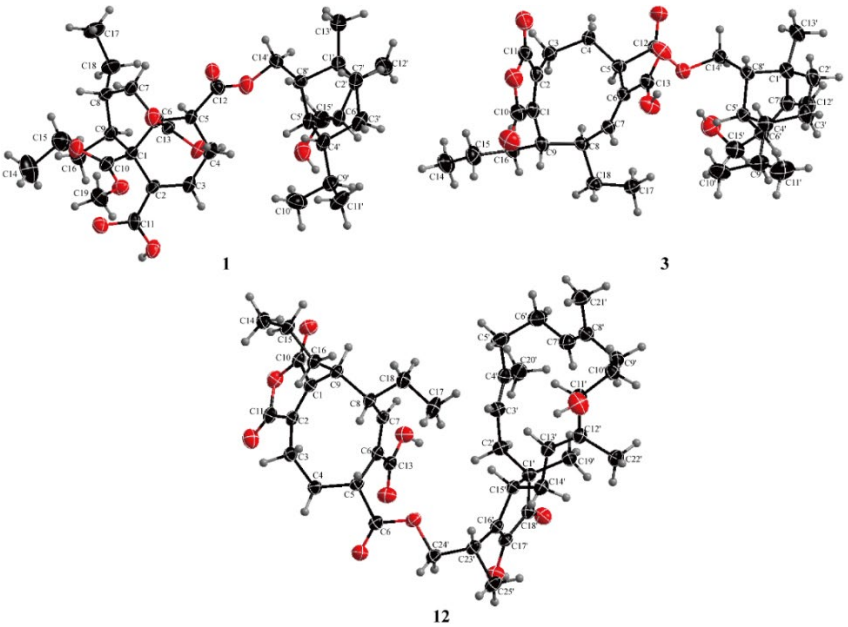

Figure 3. Single-crystal structures of **1**, **3**, and **12**.

https://doi.org/10.26434/chemrxiv-2024-g54bp **ORCID:** https://orcid.org/0000-0002-7854-8207 Content not peer-reviewed by ChemRxiv. **License:** CC BY-NC-ND 4.0

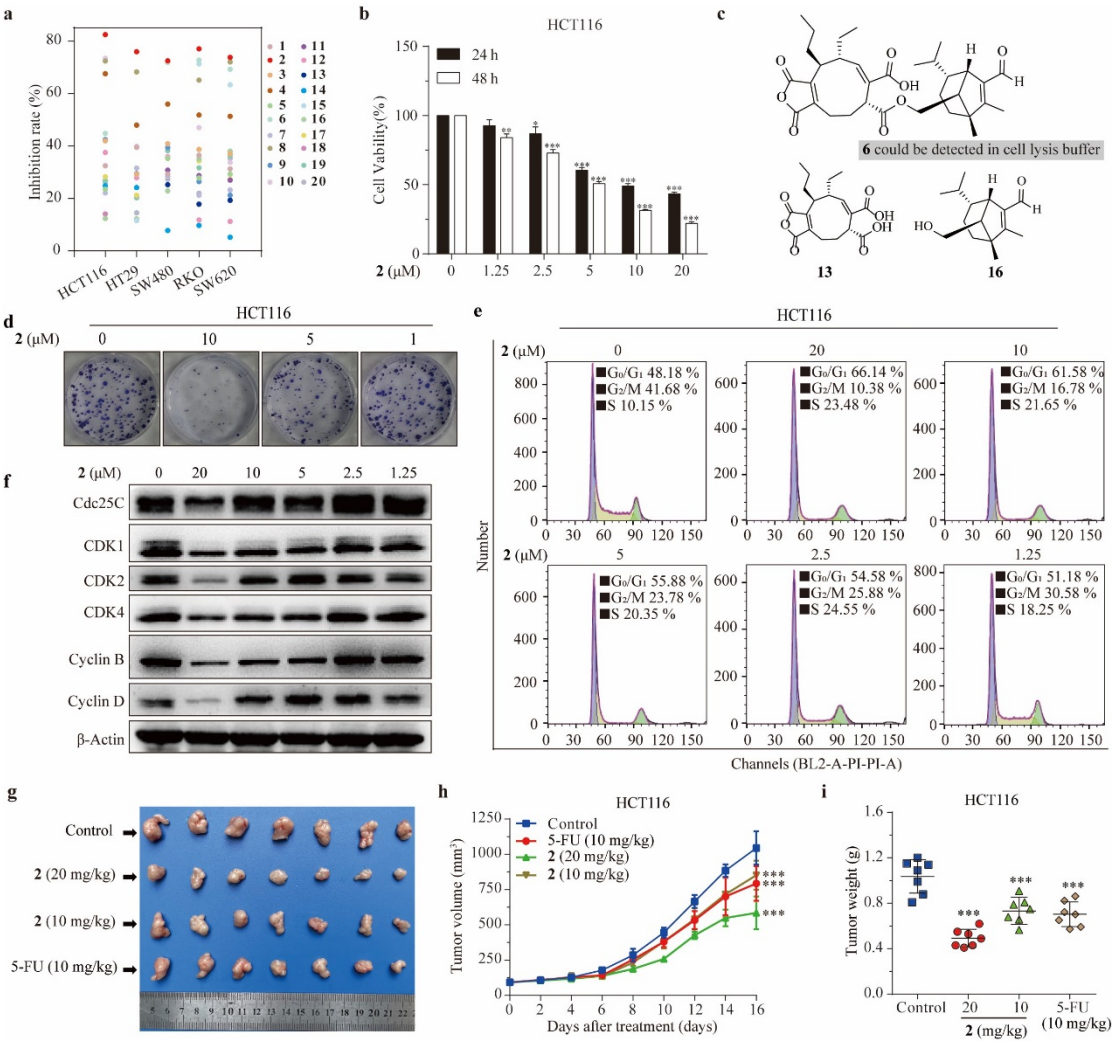

Figure 4. Compound **2** inhibits CRC cell growth *in vitro* and *in vivo*. (a) The cytotoxicity of isolated compounds against five CRC cells (10 μM, 48 h) including HCT116, HT29, SW480, RKO, and SW620 cells. (b) The cell viability of **2**-treated HCT116 cells after 24 or 48 h. The cells were exposed to various concentrations of **2** for 24 or 48 h. The cell viability was measured using the SRB assay. (c) Representative dimer structure of **6** and their monomers. (d) Representative images of colonies formed after treatment with **2**. The cells were exposed to various concentrations of **2** for 24 h and the numbers of colony were manual counted. (e) Compound **2** influenced the cell cycle in HCT116. The cell cycle was analyzed by PI staining and detected using flow cytometry. (f) Representative immunoblots showed the effect of **2** on Cdc25C, CDK1, CDK2, CDK4, Cyclin B, and Cyclin D. HCT116 cells were treated with various concentrations of **2** for 24 h, and the expressions of indicated proteins were detected using western blotting. (g) Tumors removed were photographed. Female athymic nude BALB/c mice bearing HCT116 xenograft tumors were

https://doi.org/10.26434/chemrxiv-2024-g54bp ORCID: https://orcid.org/0000-0002-7854-8207 Content not peer-reviewed by ChemRxiv. License: CC BY-NC-ND 4.0

intraperitoneally injected with various concentrations of **2** or control every other day. 5-FU (10 mg/kg) group as positive control. (h and i) The effects of **2** on the growth curves of subcutaneoue xenografts of HCT116 and the effects on the tumor weight. The results are expressed as mean ± SD of three independent experiments. * $p < 0.05$, ** $p < 0.01$, *** $p < 0.001$ vs. control.

https://doi.org/10.26434/chemrxiv-2024-g54bp **ORCID:** https://orcid.org/0000-0002-7854-8207 Content not peer-reviewed by ChemRxiv. **License:** CC BY-NC-ND 4.0

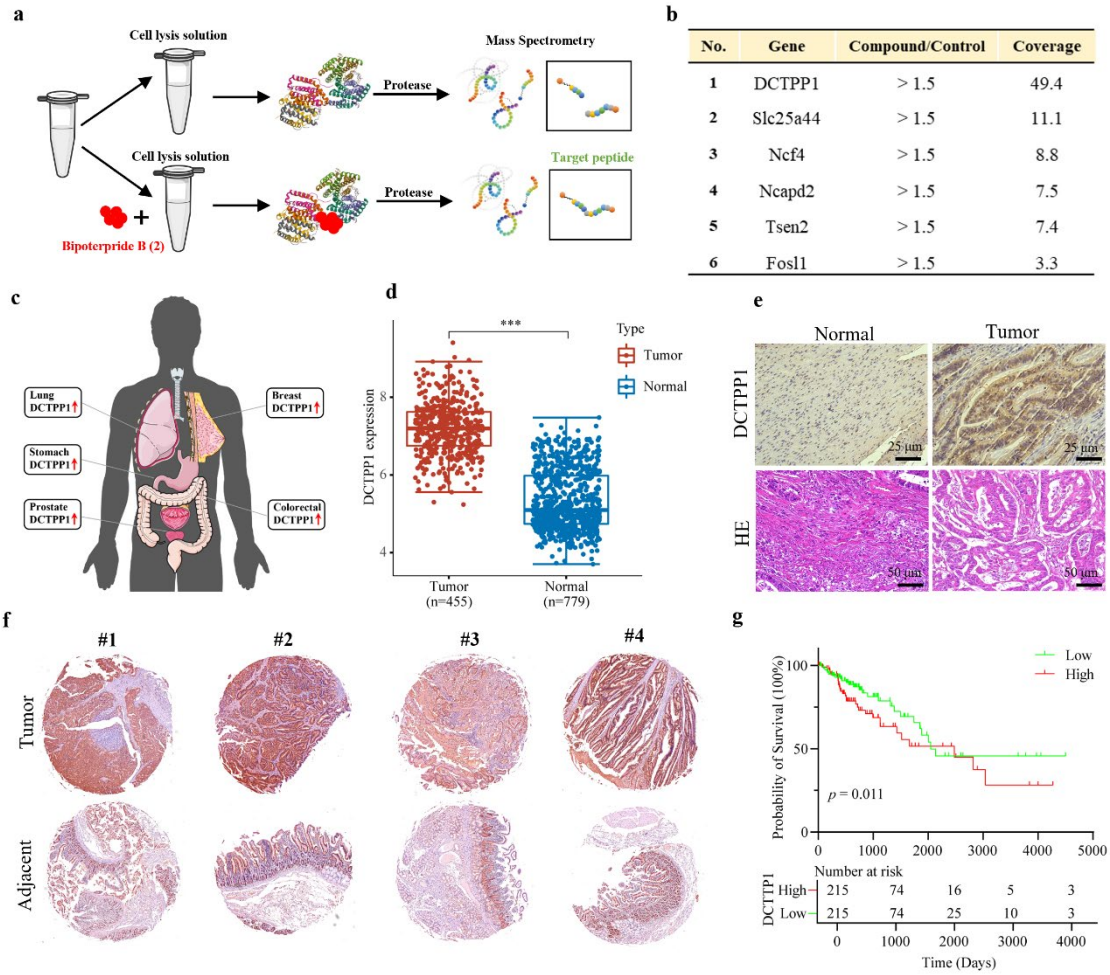

Figure 5. DCTPP1 protein contributes to the progression of CRC and is the target of **2**. (a) Overall scheme of the DARTS-based target fishing in HCT116 cells. (b) The top 6 candidate proteins identified by mass spectrometry analysis. (c) DCTPP1 is highly expressed in lung, stomach, prostate, breast, and colorectal tumors. (d) Statistic analysis of DCTPP1 expression in CRC cancer and adjacent tissues (***$p < 0.001$). (e) DCTPP1 expression levels were higher in CRC patient tissues than in normal tissues. (f) Representative IHC staining of human CRC samples from a tissue microarray. (g) Overall survival and the cumulative recurrence-free survival curves of patients with high or low expression of DCTPP1 in CRC tissues were evaluated by Kaplan–Meier curves. * $p < 0.05$, ** $p < 0.01$, *** $p < 0.001$ vs. control.

https://doi.org/10.26434/chemrxiv-2024-g54bp **ORCID:** https://orcid.org/0000-0002-7854-8207 Content not peer-reviewed by ChemRxiv. **License:** CC BY-NC-ND 4.0

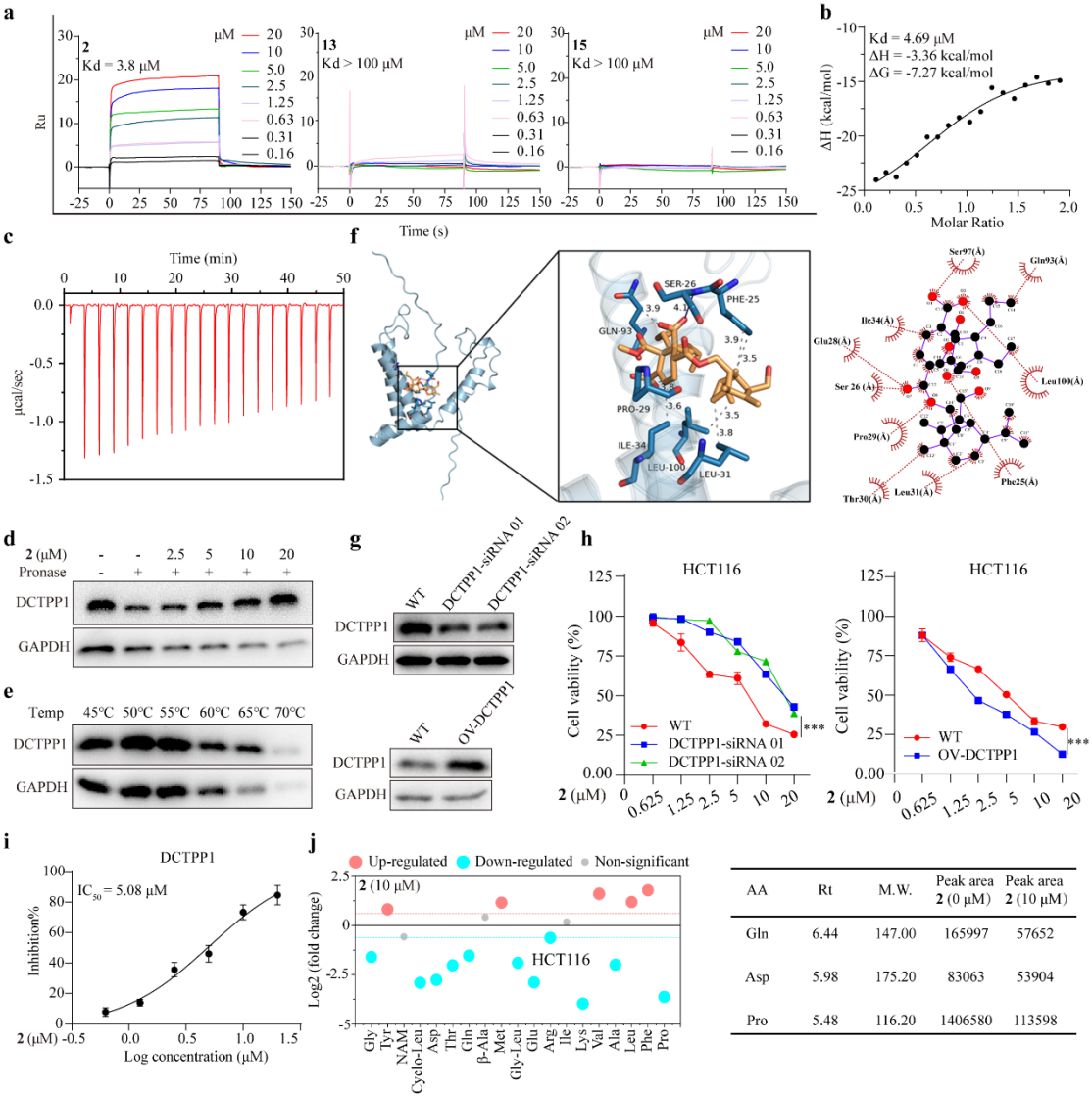

AA	Rt	M.W.	Peak area 2 (0 μM)	Peak area 2 (10 μM)
Gln	6.44	147.00	165997	57652
Asp	5.98	175.20	83063	53904
Pro	5.48	116.20	1406580	113598

Figure 6. Compound **2** exhibit anti-CRC activity through directly targeting DCTPP1 to intervene with acid metabolic reprogramming. (a) SPR analysis of interactions between **2** and DCTPP1, compound **13** and **15** were as negative control. (b and c) ITC analysis of interactions between **2** and DCTPP1. (d) DARTS analysis between **2** and DCTPP1. (e) CETSA analysis of intracellular binding between **2** and DCTPP1. Protein levels were investigated at different temperatures under the treatment of **2** (10 μM) in HCT116 cells. (f) The binding of DCTPP1 with **2** was investigated by molecular docking. (g) The western blot analysis of DCTPP1 expression in wild type, knockdown, and overexpression HCT116 cells. (h) The cell viability of **2** against WT, DCTPP1-siRNA, and OV-DCTPP1 HCT116 cells . (i) The inhibitory enzyme activity of **2** on DCTPP1 protein. (j and k) Compound **2** induce amino acid reprogramming and reduce the content of amino acids in HCT116 cells. *** $p < 0.001$ vs. control

https://doi.org/10.26434/chemrxiv-2024-g54bp **ORCID:** https://orcid.org/0000-0002-7854-8207 Content not peer-reviewed by ChemRxiv. **License:** CC BY-NC-ND 4.0